fibers run under the epicardium side of the left ventricular myocardium from base to apex (2), which indicate that a subendocardial myocardial infarction that spared the epicardium do not interrupt the sympathetic transmission (9). Reinnervation is reported to occur in the peri-infarcted area after transmural myocardial infarction in experimental animal studies and in humans (1–4), but there is no report of a reinnervation phenomenon in the infarcted area. The denervation results from interruption of normal neural transmission in postganglionic sympathetic nerve coursing through the area of infarction. However, our patient had good collateral vessels, and successful direct percutaneous transluminal coronary angioplasty was achieved in the early hours of myocardial infarction, which resulted in a relatively small ^{201}Tl defect size. Left ventricular asynergy of the anterior and septal walls improved, and the electrocardiogram showed increase of R waves in the V1-V4 leads at 12 mo, which suggests the presence of viable myocardium in the infarcted area. Moreover, coronary angiography at 12 mo showed a patent left anterior descending artery. Therefore, one of the causes of reinnervation in our patient was a brief length of sympathetic fiber interruption.

Zipes et al. (2) found that preconditioning ischemia preserves the efferent sympathetic response during the first hour of subsequent sustained ischemia. In addition to early reperfusion, repeated episodes of ischemia before the onset of myocardial infarction in our patient could have protected the adrenergic nerve to be more resistant to ischemia. Therefore, initial damage of [^{123}I]MIBG uptake after myocardial infarction might have been due to the functional derangements of nerve action rather than the structural damage.

There is less attenuation of 159 keV (^{123}I) compared to 80 keV (^{201}Tl). Therefore, some of the difference between [^{123}I]MIBG and ^{201}Tl defects at 12 mo may be explained by differential attenuation. However, because ^{201}Tl defects were in the midportion of the anterior and septal walls, in addition to the patient's small size, indicate that attenuation effects were not significant.

CONCLUSION

Reinnervation can occur not only in the peri-infarcted area but also in the infarcted area.

REFERENCES

1. Minardo JD, Tuli MM, Mock BH, et al. Scintigraphic and electrophysiological evidence of canine myocardial sympathetic denervation and reinnervation produced by myocardial infarction or phenol application. *Circulation* 1988;78:1008–1019.
2. Zipes DP. Ischemic modulation of myocardial innervation. *G Ital Cardiol* 1992;22:615–621.
3. Hartikainen J, Kuikka J, Mäntysaari M, Länsimies E, Pyörälä K. Sympathetic reinnervation after acute myocardial infarction. *Am J Cardiol* 1996;77:5–9.
4. Mitrani R, Burt RW, Klein LS, et al. Regional cardiac sympathetic denervation and reinnervation following myocardial infarction in humans [Abstract]. *Circulation* 1992;86(suppl I):1-247.
5. Kline RC, Swanson DP, Wieland DM, et al. Myocardial imaging in man with I-123-metaiodobenzylguanidine. *J Nucl Med* 1981;22:129–132.
6. Rentrop KP, Cohen M, Blanke H, Phillips RA. Changes in collateral channel filling immediately after controlled coronary artery occlusion by an angioplasty balloon in human subjects. *J Am Coll Cardiol* 1985;5:334–340.
7. Sisson JC, Wieland DM, Sherman P, Mangner TJ, Tobes MC, Jacques S Jr. Metaiodobenzylguanidine as an index of the adrenergic nervous system integrity and function. *J Nucl Med* 1987;28:1620–1624.
8. Dae MW, Marco TD, Botvinick EH, et al. Scintigraphic assessment of MIBG uptake in globally denervated human and canine hearts—implications for clinical studies. *J Nucl Med* 1992;33:1444–1450.
9. Inoue H, Zipes DP. Results of sympathetic denervation in the canine heart: supersensitivity that may be arrhythmogenic. *Circulation* 1987;75:877–887.

Compartment Model for Measuring Myocardial Oxygen Consumption Using [1-^{11}C]Acetate

Karl T. Sun, Kewei Chen, Sung-Cheng Huang, Denis B. Buxton, Herbert W. Hansen, Anatole S. Kim, Stefan Siegel, Yong Choi, Peter Müller, Michael E. Phelps and Heinrich R. Schelbert

Division of Nuclear Medicine, Department of Molecular and Medical Pharmacology, UCLA School of Medicine; Laboratory of Structural Biology and Molecular Medicine, University of California, Los Angeles, California

Although [1-^{11}C]acetate has been validated as a PET tracer for myocardial oxygen consumption (MVO$_2$) in animals and humans, mono- and biexponential fitting of the tissue time-activity curve yields only estimates of MVO$_2$. This study attempts to develop and validate a simple tracer kinetic model in vivo for estimation of regional MVO$_2$. **Methods:** Twenty-seven experiments were performed in 12 anesthetized dogs with [1-^{11}C]acetate and serial PET images under different MBF and MVO$_2$ (baseline, ischemia, xylazine, dobutamine and dipyridamole). Estimates of MVO$_2$ were obtained from dynamic [1-^{11}C]acetate PET and model fitting. MBF was measured by radiolabeled microspheres, and MVO$_2$ was calculated by the Fick method using arterial and coronary blood samples. **Results:** The proposed model fitted equally well for all study conditions with a multiple correlation coefficient of 0.985 ± 0.026. Estimated MVO$_2$ correlated linearly with measured MVO$_2$ (y = 0.033 + 0.690x, r = 0.92, s.e. of estimates = 0.020). **Conclusion:** This study indicates that MVO$_2$ can be assessed with PET and [1-^{11}C]acetate over a wide range with a simple tracer kinetic model.

Key Words: positron emission tomography; [1-^{11}C]acetate; myocardial oxygen consumption

J Nucl Med 1997; 38:459–466

Carbon-11-acetate has been extensively validated as a PET tracer for the noninvasive assessment of regional myocardial oxidative metabolism (1–5). It has been shown that myocardial oxygen consumption (MVO$_2$) can be estimated by either monoexponential fitting of the linear portion or by biexponential fitting of the entire clearance curve of [1-^{11}C]acetate clearance (2). Although simple, this approach has several potential limitations: (a) only an index of oxidative metabolism, rather than the absolute substrate flux, can be obtained; (b) the distribution of the arterial input function, spillover from myocardium to bloodpool and recirculation of labeled acetate are not taken into account (6,7); and (c) estimates are affected by

the choice of the data points on the tissue time-activity curve and are less accurate in studies with noise.

A comprehensive tracer kinetic model has been developed and validated biochemically in isolated perfused rat hearts for the estimation of MVO_2 using $[1\text{-}^{11}C]$acetate (8). However, the statistical noise in the PET data limits the number of compartments that can be used in the clinical environment. It was, therefore, the purpose of this study to simplify the previously established comprehensive tracer compartment model for $[1\text{-}^{11}C]$acetate and to evaluate its in vivo applicability in acute dog experiments for the estimation of regional MVO_2, with the ultimate goal to apply it in humans.

MATERIALS AND METHODS

Animal Preparation

Twelve mongrel dogs weighing 22 to 37 kg (mean 28 ± 5 kg) were studied. The animals were anesthetized with intravenous sodium thiomylal (15–20 mg/kg). The dogs were intubated and ventilated with room air by a Harvard respirator (South Natick, MA). Anesthesia was maintained by additional intravenous sodium thiomylal as needed. A number 7 French pigtail catheter was inserted into the left ventricle through a sheath from the femoral or carotid artery for arterial blood sampling and injection of radiolabeled microspheres. An additional catheter was advanced from the femoral artery into the abdominal aorta for blood pressure monitoring or withdrawal of reference blood samples to calculate myocardial blood flow with the microsphere technique (9). The left jugular vein was dissected free and a number 7 French Sones catheter was advanced through a sheath into the coronary sinus under fluoroscopic guidance. Arterial blood pressure and electrocardiogram were monitored continuously on a strip chart recorder.

PET Imaging

$[1\text{-}^{11}C]$acetate was synthesized using a modified procedure of Pike et al. (10). Imaging was performed with a whole-body tomograph. This scanner acquires simultaneously 15 planes with an interplane spacing of 6.75 mm. The tomograph's gantry was rotated horizontally to $-15°$ in order to align the tomograph's axis with the long axis of the dog heart and to minimize the angle of reorientation. A rectilinear scan was obtained for correct positioning of the dog, followed by a 20-min transmission scan with a ^{68}Ge ring source for subsequent correction of photon attenuation. Acquisition of the emission images commenced 5 sec before injection of $[1\text{-}^{11}C]$acetate to ensure recording of the entire input function. An average of 20 mCi $[1\text{-}^{11}C]$acetate was dissolved in 10 ml 0.9% saline solution (pH 7.4, 308 mOsmole/liter), injected intravenously with an infusion pump as a bolus spread over 15 sec and flushing the catheter with 0.9% saline solution for another 15 sec. The image acquisition sequence was as follows: 12 images of 10 sec each followed by eight images of 30 sec each, four images of 60 sec each, two images of 500 sec each and two images of 600 sec each, resulting in a total acquisition time of 40 min.

Study Subgroups

Eight baseline studies were performed in eight dogs. To examine the validity of the simplified tracer compartment model over a wider range of MBF and MVO_2, the following interventions were performed.

Changes in Cardiac Work. In four experiments in four dogs, cardiac workload was increased by infusing dobutamine (Dobutrex®, Eli Lilly Industries, Carolina, Puerto Rico) intravenously at a rate of 5–10 μg/kg/min throughout the study. Cardiac work was lowered in five experiments in four dogs by intravenous bolus injection of 0.5–1.0 mg/kg xylazine (Rompun®, Mobay Corporation Shawnee, KS), a parasympathomimetic general anesthetic agent.

Reduced Myocardial Blood Flow. In three experiments in two dogs, myocardial blood flow was reduced regionally. In addition to the animal instrumentation described above, the following preparations were made on these dogs to reduce MBF. After a left thoracotomy, the pericardium was widely incised and sutured to the chest wall forming a cradle suspending the heart. After dissecting the proximal left descending artery (LAD), an external balloon occluder was placed around the vessel. The balloon was then slowly inflated with air by using a 1-ml plastic syringe. The perfusion pressure distal to the site of the occlusion was monitored with a pressure transducer, connected via a plastic tube to a 25-gauge needle that was inserted into the LAD distal to the occlusion site. The coronary occlusion was adjusted continuously in order to maintain the distal coronary pressure reduced at a constant level of 15%–20% below the baseline pressure. A fine catheter (Tygon®, inner diameter 1.8 mm, Norton Performance Plastics, Akron, OH) was placed into the cardiac vein draining the hypoperfused territory to obtain venous blood for blood gas analysis.

Hyperemia. To test the tracer compartment model in the high-flow range when MBF is uncoupled from MVO_2, and thus to prove the independence of the model parameters for MBF and MVO_2, in four experiments in four dogs, dipyridamole (Persantine®, Boehringer Ingelheim Pharmaceuticals, Ridgefield, CT) was continuously infused intravenously at a rate of 0.15 mg/kg/min throughout the study, starting 15 min before the scan.

Measurement of Myocardial Blood Flow

Radiolabeled carbonized polystyrene microspheres (DuPont, North Billerica, MA, 15.5 ± 0.1 μm in diameter, suspended in 10% dextran with one drop of Tween 80) were resuspended with a vortex shaker and mixed with 3 ml heparinized blood. Shortly before the start of the scan, approximately 2×10^6 microspheres labeled with ^{46}Sc, ^{57}Co., ^{95}Nb, ^{103}Ru or ^{113}Sn were injected into the left ventricle. Arterial blood was withdrawn with a Harvard infusion pump at a rate of 7.8 ml/min for 2 min. At the end of each study, the dog was killed with Surital and concentrated KCl injected into the left ventricle. The heart was excised and the entire left ventricle was cut into pieces of approximately 1 g each. The activity concentration of the myocardial tissue samples and the activity in the arterial reference sample were determined in a well counter. Myocardial blood flow was calculated as described previously (9) and is given as the mean value of all tissue samples in each experiment except for those studies with regional MBF decreases. In these experiments, the hypoperfused region was delineated by injecting gentian violet into the left ventricle after complete inflation of the balloon occluder, thus leaving the hypoperfused area distal to the occlusion site unstained.

Metabolic Measurements

Hemoglobin, hematocrit and blood gases were measured in all 24 studies immediately before injection of $[1\text{-}^{11}C]$acetate and 20 min thereafter. Blood gases were measured with a Corning Model 168 blood gas analyzer (Corning Inc., Corning, NY). Serum levels of glucose, lactate and free fatty acids were determined at the same time points in 20 studies by methods described previously (11). Myocardial oxygen consumption (ml/g/min) and substrate consumptions were calculated by the Fick principle from the arteriovenous differences across the heart, hematocrits and myocardial blood flows measured by microspheres (12).

In the ischemic studies, regional MVO_2 in the territory of the LAD was calculated from the differences in oxygen saturation between arterial blood and venous blood from the anterior interventricular vein. The mean values of two measurements, 20 min apart, were used. Regional MBF was obtained by counting the

tissue samples from the territory supplied by the LAD beyond the occlusion.

Measurements of Carbon-11-Labeled Carbon Dioxide and Non-Carbon Dioxide Components in Blood

Blood samples (1.0–1.5 ml each) from the left ventricle were drawn every 10 sec during the first 2 min after [1-^{11}C]acetate injection, then at 1-min intervals for the following 4 min, at 2-min intervals for the next 16 min and every 5 min for an additional 10 min. Because of the low blood flow in the coronary sinus, only six samples (1.0–1.5 ml each) during the first 2 min were obtained. Thereafter, the sampling rate was the same as that from the left ventricle.

The exact weights of the blood samples were determined by weighing the flasks before and after they were filled with blood. Labeled CO_2 was determined by acidification of 1 ml of arterial and coronary sinus blood samples with 0.5 ml of acetic acid (2 M, pH 3.3) in a sealed Erlenmeyer flask. Labeled CO_2 was trapped in a center well filled with 0.3 ml of phenylethylamine (13) after shaking for 45 min at room temperature. An aliquot of the remaining ^{11}C activity in the flask representing non-CO_2 ^{11}C components, was also counted. The bicarbonate recovery was 96%.

Measurement of Amino Acids, TCA Cycle Intermediates and Acetate

The model approach requires the exact knowledge of the [1-^{11}C]acetate input function. In order to determine the content of labeled metabolites and acetate in left ventricular blood at different time points, a second series of four studies in two additional dogs (two studies per dog) was performed (two baseline, one dobutamine and one xylazine study). A total of 11 blood samples was obtained over a period of 10 min at 0.5, 1.0, 1.5, 2.0, 2.5, 3.0, 4.0, 5.0, 6.0, 8.0, 10.0 min after intravenous administration of [1-^{11}C]acetate.

Acetate was separated from amino acid and TCA cycle metabolites as described previously (14). In brief, whole blood (1 ml) was deproteinized with cold $HClO_4$, neutralized and placed on a combined column of 2 ml Dowex 1 (formate form) on top of 2 ml Dowex 50 (H+ form). The column was washed with 6 ml water to elute nonionized species, and then with 10 ml 0.25 M formic acid, which elutes acetate and ketone bodies, leaving amino acid and TCA cycle metabolites behind. The washes and activity remaining on the column were then determined by counting in a gamma counter, with appropriate corrections for physical decay of activity. [1-^{14}C]acetate trapping on column was 98.5% and recovery washing 97.3%, β-hydroxybutyrate trapping was 100% and recovery washing 75% (spectrophotometric assay).

PET Image Analysis

The PET image files were reconstructed on a VAX 4000 mainframe computer (Digital Equipment Corporation, Maynard, MA) using a Shepp-Logan filter with a cutoff frequency of 0.15 cycles/cm. The images were transferred to a Macintosh IIfx desktop computer (Apple Computer, Inc., Cupertino, CA) and reoriented into six short-axis cuts as described previously (15). The reslicing parameters derived from an image frame at approximately 2 min after tracer injection, when the myocardium is best visualized, were then applied to all serially acquired image frames of the study. Eight 45° sectorial ROIs were assigned to each of three midventricular planes and were copied to all serially acquired and reoriented images. Time-activity curves were then derived from each sector and corrected for partial volume effect using a previously validated profile fitting approach (16). In the ischemic studies, one ROI in the center of the hypoperfused area and a large control ROI in normally perfused myocardium were drawn. Each tissue time-activity curve was corrected for physical decay. An
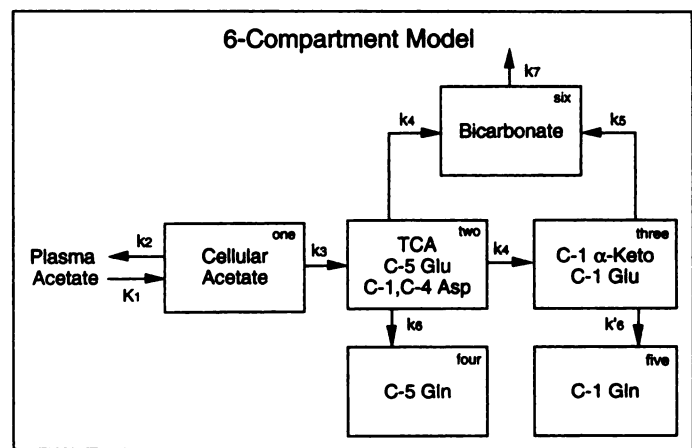

FIGURE 1. Configuration of a six-compartment model for [1-^{11}C]acetate kinetics that has been previously validated in isolated perfused rat hearts. The rate constant k_4 reflects the oxidative flux through the TCA cycle and was used to estimate myocardial oxygen consumption (MVO_2). Glu = glutamate; Asp = aspartate; Keto = ketoglutarate; Gln = glutamine.

average tissue time-activity curve was then generated from the regional time-activity curves derived from the three planes.

Comparison of the arterial input function by direct arterial blood sampling to the input function derived from an ROI within the left ventricle of the PET images required a calibration factor which was obtained by scanning a cylinder phantom containing ^{68}Ge (17).

Tracer Kinetic Model for [1-^{11}C]Acetate

The term compartment model refers to a set of functional compartments that lumps biochemical pools together rather than to a description of cellular organization.

A six-compartment model, previously developed and validated in isolated perfused rat hearts (Fig. 1 (8)), was simplified to a two-compartment model (Fig. 2). Although the complex six-compartment model describes the metabolic fate of radiolabeled acetate comprehensively, it is error sensitive and its use is impractical and time consuming. Therefore, simplification is necessary.

By using the initial 5 to 10 min after administration of [1-^{11}C]acetate for data analysis, several simplifications can be made as described below (Fig. 1):

Since labeled glutamine concentrations remain relatively low in both normoxia and ischemia during the first 10 min after administration of labeled acetate compared to the glutamate concentration, we assumed the flux from glutamate to glutamine to be negligible. Also, labeled bicarbonate concentrations were found to be relatively constant in the isolated perfused rat hearts, and k_7 was much larger than k_4 and k_5. Therefore, Pools 4, 5 and 6 can be ignored without significant influence on the estimation.

We further found that activity in Pool 1 cleared rapidly and was consistently very low compared to the activity in Pool 2. This
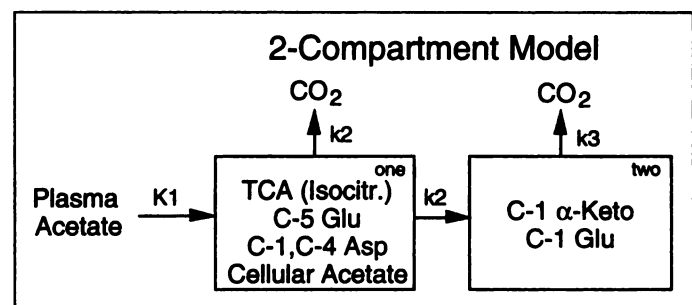

FIGURE 2. Configuration of the simplified two-compartment model. K 1 denotes the extraction of labeled acetate from the vascular space into the cell and k_2 in the two-compartment model (k_4 in the six-compartment model) reflects mainly the turnover rate of the glutamate pool through the TCA cycle.

TABLE 1
Hemodynamic Parameters, MBF and MVO$_2$

Parameter	Control (n = 8)	Dobutamine (n = 4)	Xylazine (n = 5)	Dipyridamole (n = 4)	Occlusion (n = 3)	Occlusion ischemic (n = 3)
Heart rate (bpm)	165.8 ± 15.9	169.8 ± 52.1	94.6 ± 24.8	122.3 ± 37.3	165.0 ± 19.1	165.0 ± 19.1
Systolic BP (mmHg)	172.4 ± 22.1	158.8 ± 43.2	131.0 ± 20.3	122.8 ± 39.8	154.3 ± 27.3	154.3 ± 27.3
Rate pressure product (mmHg × bpm)	28717 ± 5630	29351 ± 9527	12110 ± 2500	15788 ± 9272	25577 ± 5872	25577 ± 5872
Myocardial blood flow (ml/g/min)	1.40 ± 0.35	1.93 ± 1.12	0.74 ± 0.18	5.00 ± 2.35	1.08 ± 0.18	0.74 ± 0.55
Myocardial oxygen consumption (ml/g/min)	0.182 ± 0.052	0.212 ± 0.099	0.086 ± 0.02	0.083 ± 0.06	0.124 ± 0.018	0.085 ± 0.059

allowed further simplification to a two-compartment model by merging Pools 1 and 2 into one pool. K1 in this model denotes the extraction of labeled acetate from the vascular space into the cell. The rate constant k$_2$, which denotes the production rate of CO$_2$ and C-1 α-ketoglutarate, reflects the oxidative flux through the TCA cycle. This two-compartment model was eventually used for all studies. The results reported below relate to this model.

Model Estimation of MVO$_2$

In the two-compartment tracer kinetic model, Compartment 1 (excluding intracellular acetate) represents the amount of substrate available for oxid ation through the TCA cycle. For simple first-order processes, the flux can be determined as the product of the amount of substrate in a compartment and the transfer rate constant of the corresponding compartment.

MVO$_2$ was estimated using the following equation that has been proposed by Ng et al. (8). Tissue concentrations of labeled glutamate, aspartate and TCA-cycle intermediates corrected for wet weight obtained from isolated perfused rat hearts were used to estimate MVO$_2$. The wet weight was calculated by multiplying the dry weight by 5.64 (8).

$$MVO_2 = 6*k_2*([Glu] + [Asp] + [TCA]) \cdot$$

The factor 6 is the product of three terms, as follows. The rate constant k$_2$ is multiplied by 2 to account for the fact that CO$_2$ and C-1 α-ketoglutarate are produced at the same rate in Compartment 1. A further factor of 1.5 accounts for the fact that approximately 2/3 of oxygen consumption occurs during TCA-cycle oxidation. A final factor of 2 accounts for the two molecules of oxygen which are utilized per turn of the cycle.

Model Fitting

The model fitting was performed on a Macintosh IIfx desktop computer (Apple Computer, Inc., Cupertino, CA) using a custom-developed toolbox based on the Matlab® 3.5 program (Mathwork Inc. Natick, MA). The constrained SQP (sequential quadratic programming) optimization procedure was used for the nonlinear fit (18). The tissue time-activity curves were fitted with the two-compartment model over 5 min for studies at baseline, during dipyridamole and dobutamine and over 10 min for studies after administration of xylazine and under ischemia. Selection of these time periods for model fitting were based on the following considerations. First, the activity of labeled CO$_2$ in coronary sinus blood reached its peak at around 3 to 4 min for studies at baseline and during dipyridamole and dobutamine but between 7 and 8 min in the ischemic and xylazine studies. Therefore, the fitting period included the time of the peak CO$_2$ efflux. Second, the above-mentioned model simplifications are only valid for this time period. We found that fitting over longer time periods prolongs the analysis without improving significantly the results.

Because the compartment model describes the biochemical changes less reliably very early after tracer injection (negligible concentrations of labeled metabolites and amino acids) and because of the higher noise level in the early measurement points, less weight was given to the data points of the first 2 min. The relation of 1:20 (data points in the first 2 min were given 20 times less weight) was determined empirically. Howevethethether, it should be emphasized that the sensitivity of the results to weighting is low, in other words, different weighting did not yield significantly different estimates.

The arterial input function was derived in this study from blood samples collected directly from the left ventricle after correction for labeled CO$_2$, metabolites and amino acids. Two additional parameters, spillover and time delay (time shift between measured input and the true, nonobservable one) were estimatethed simultaneously with the rate constants of the two-compartment [1-^{11}C]acetate model (Fig. 2), as published previously (19).

Statistical Analysis

Values are expressed as mean ± s.d. Paired and unpaired t-test was used as appropriate for comparisons. Differences with p values < 0.05 were considered statistically significant. Stepwise regression was used to compare the relationship between arterial substrate levels or consumption and first pass extraction fraction of

TABLE 2
Arterial Substrate Concentrations and Consumption

Intervention	Arterial concentration			Substrate consumption		
	Glucose (mg/dl)	Lactate (mg/dl)	Free fatty acid (mEq/liter)	Glucose (mg/100 g/min)	Lactate (mg/100 g/min)	Free fatty acid (mmole/100 g/min)
Baseline	101.1 ± 7.4	13.0 ± 4.6	0.198 ± 0.560*	7.64 ± 4.55	4.74 ± 2.45	0.064 ± 0.019
Dobutamine	130.9 ± 37.1	21.7 ± 11.1	0.955 ± 0.145	7.16 ± 7.93	4.35 ± 4.28	0.267 ± 0.110
Xylazine	113.9 ± 9.1	10.3 ± 2.4	0.200 ± 0.119*	5.76 ± 2.80	2.18 ± 1.33†	0.027 ± 0.130*
Dipyridamole	109.4 ± 1.6	11.8 ± 5.3	0.199 ± 0.151	7.08 ± 2.55	1.20 ± 0.47	0.078 ± 0.048

*p < 0.05 Concentration: baseline and xylazine vs. dobutamine; consumption: xylazine vs. baseline.
†p < 0.01 Consumption: xylazine vs. baseline.
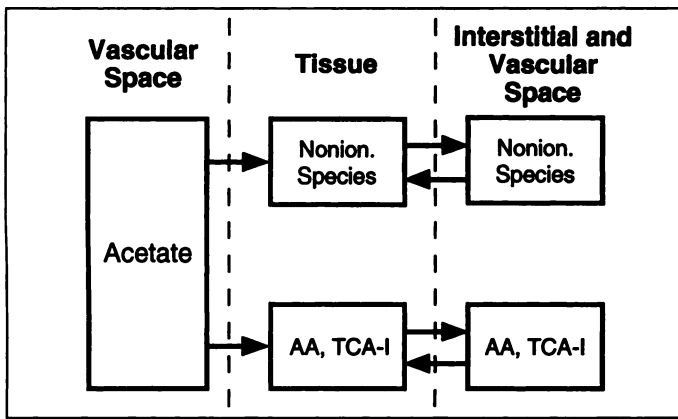
FIGURE 3. Model configuration that accounts for the conversion of [1-^{11}C]acetate to its metabolites (other than CO_2) in plasma. Labeled acetate enters the tissue and is metabolized to labeled CO_2 and labeled non-CO_2 metabolites. Some labeled non-CO_2 metabolites leave the cell into interstitium or backdiffuse into the vascular space.

[1-^{11}C]acetate. A χ^2-test was used to analyze the goodness of fit by the kinetic model to the measured tissue time-activity curve (20,21) and the nonparametric run test was used to test whether the data points about the fitted curve were randomly distributed about the fitted curve (22). The Durbin-Watson test for autocorrelation was applied and the Cochrane-Orcutt procedure was used to correct for the autocorrelated error terms for the regression between measured and estimated MVO_2 values (23).

RESULTS

Hemodynamic and Metabolic Parameters

Hemodynamic and metabolic findings for the baseline and the intervention studies are summarized in Tables 1 and 2. The absence of a significant difference between the rate pressure products of the baseline and the dobutamine studies is explained by the way the dogs were selected. In order to get the greatest change in cardiac workload possible, dogs with lower rate pressure products (i.e.,< 21,000 mmHg/min^{-1}) were chosen for dobutamine studies whereas several dogs with high rate pressure products at baseline were selected for an intervention with xylazine. Despite the lack of such significant differences, the interventions nevertheless were meaningful as they offered
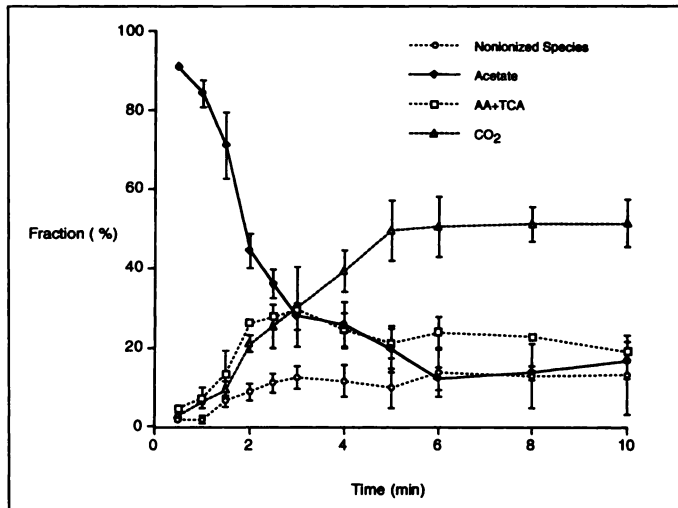
FIGURE 4. Time-activity curves of CO_2-labeled acetate with ketone bodies, nonionized species (predominantly glucose and cholesterol) and amino acids and TCA-cycle intermediates expressed as fractions of the total measured activity in arterial blood during the first 10 min after administration of [1-^{11}C]acetate.
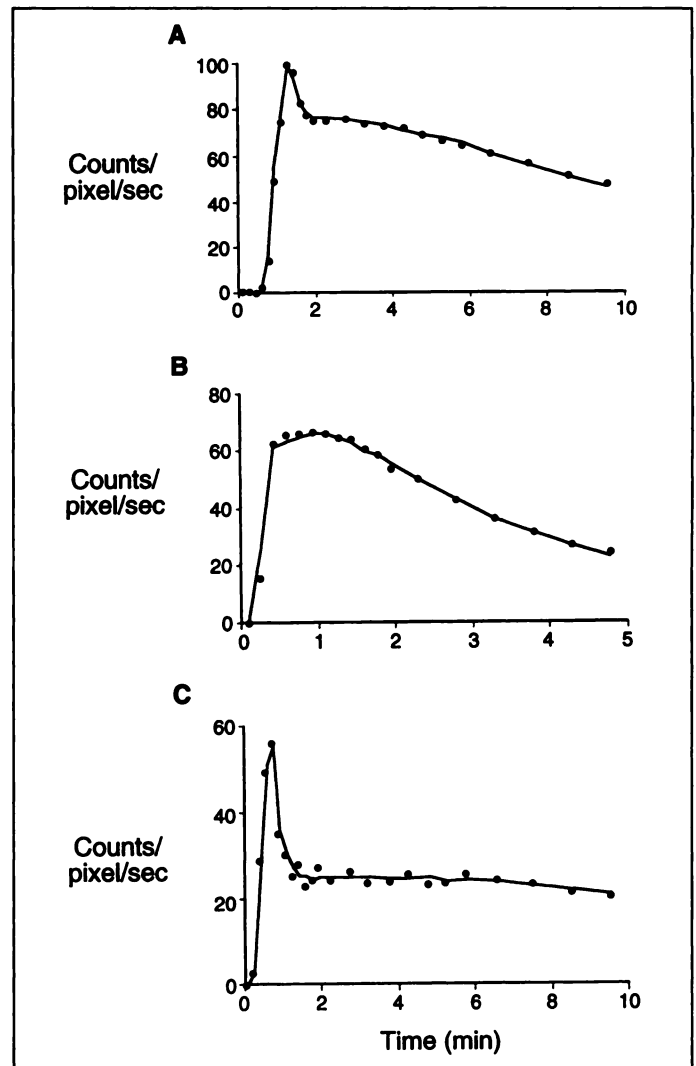
FIGURE 5. Correlation between measured total tissue activity by PET and model fitting from a (A) xylazine, (B) dobutamine and (C) occlusion study. The mean multiple correlation coefficient r of the fitting was 0.985 ± 0.026.

the possibility to examine whether the model appropriately tracked directional changes. The mean rate pressure product in the studies without any intervention was 28,717 ± 5630 mmHg/min^{-1}. In the dobutamine group, the rate pressure product increased from 20,279 ± 8181 at baseline to 29,351 ± 9527 mmHg/min^{-1} (p = 0.008) during dobutamine, whereas the rate pressure product fell from 27,220 ± 3731 to 12,110 ± 2500 mmHg/min^{-1} (p = 0.005) in the xylazine group.

Table 2 shows arterial substrate concentrations and substrate consumption (glucose, lactate, free fatty acid). Free fatty acid concentrations at baseline and with xylazine were significantly lower compared to those with dobutamine (p < 0.05). With

TABLE 3
MBF, Uptake Fractions and r-Values Curve Fit

Intervention	MBF (ml/g/min)	Uptake fraction (%)	r-Value curve fit
Baseline (n = 11)	1.31 ± 0.33*	87.9 ± 10.6*	0.993 ± 0.006
Dobutamine (n = 4)	1.94 ± 1.13*	64.8 ± 13.8	0.993 ± 0.004
Xylazine (n = 5)	0.74 ± 0.18*	88.1 ± 13.8*	0.968 ± 0.045
Dipyridamole (n = 4)	5.00 ± 2.35	36.9 ± 16.9	0.992 ± 0.006
Occlusion (n = 3)	0.74 ± 0.55*	70.3 ± 25.7	0.967 ± 0.046

*p < 0.05 vs. dipyridamole.

TABLE 4
Rate Constant (k_2), Spillover and Delay

Parameter	Control (n = 8)	Dobutamine (n = 4)	Xylazine (n = 5)	Dipyridamole (n = 4)	Occlusion control (n = 3)	Occlusion ischemic (n = 3)
k_2	0.220 ± 0.064	0.260 ± 0.085	0.123 ± 0.018*	0.179 ± 0.054	0.136 ± 0.008*	0.086 ± 0.004*
Spillover (%)	30 ± 4	27 ± 3	29 ± 6	24 ± 2	31 ± 5	25 ± 3
Delay (min)	0.28 ± 0.08	0.31 ± 0.07	0.21 ± 0.06	0.28 ± 0.04	0.33 ± 0.03	0.21 ± 0.03

*$p < 0.05$ vs. control and dobutamine.

xylazine, lactate and free fatty acid consumption were significantly lower compared to baseline. The uptake fraction of [1-^{11}C]acetate obtained by model estimation was not correlated to substrate levels (lactate, free fatty acid) in arterial blood and their consumption. Furthermore, no significant relationship was found between substrate levels and consumption.

The Arterial Input Function

The total ^{11}C activity in arterial blood was found to consist of labeled CO_2, acetate, metabolites and TCA-cycle intermediates. Thus, the true input function can be calculated by total ^{11}C activity minus the sum of $^{11}CO_2$, labeled metabolites and TCA-cycle intermediates.

According to the biochemical assay procedure, three different groups of labeled metabolites of [1-^{11}C]acetate were separated from plasma: (a) labeled CO_2, (b) nonionized labeled species (such as glucose and cholesterol) and (c) labeled amino acids and TCA-cycle intermediates. In our studies, the labeled CO_2 content is measured at the same intervals as the total plasma ^{11}C activity. Thus, the non-CO_2 activity curve can be obtained by subtracting the CO_2 activity from the total measured activity. Since it is impractical to measure all labeled non-CO_2 metabolites dynamically (i.e., in short time intervals), a compartment model approach (Fig. 3) was used to recover the time course of labeled non-CO_2 metabolites and TCA-cycle intermediates (24). In brief, this model describes the dynamic distribution of labeled non-CO_2 metabolites in tissue, interstitium and vascular space. These data are derived from a second series of four studies in two dogs (two baseline, one dobutamine, one xylazine) and were used to obtain the true arterial input function for all studies.

Figure 4 shows the [1-^{11}C]acetate content in arterial blood (expressed as percentage of the non-CO_2 portion) and the distribution of the different labeled metabolites of the non-CO_2 fraction during the first 10 min after tracer administration. As the concentration of [1-^{11}C]acetate declines steadily, the concentration of nonionized species, amino acids and TCA-cycle intermediates increases over time until they reach a plateau after about 6 min. Although no serial measurements were performed in the dipyridamole and ischemic studies, the fraction of [1-^{11}C]acetate in arterial blood was measured in all studies at 2.5 min after tracer injection. There were no significant differences between the various study conditions.

Validation of the Tracer Kinetic Model

The previously developed comprehensive six-compartment model has been biochemically validated in isolated perfused rat hearts (8). The validation of the simplified two-compartment model was based on the following main criteria: (a) the curve fitting to the tissue time-activity curve is statistically satisfactory—in other words, there was no systemic error left; (b) the estimated tissue activities of the labeled metabolites and TCA-cycle intermediates are qualitatively and dynamically consistent with the measurements obtained previously from isolated rat

hearts (8); and (c) absolute values for measured and estimated MVO_2 correlate closely.

Figure 5 depicts three examples of the fitting between measured and model predicted time-activity curves for baseline, dobutamine (increased workload) and xylazine (decreased workload). As listed in Table 3, the model fits were equally good for low and high MVO_2 as well as for ischemia and hyperemia. In all studies, very high multiple correlation coefficients (mean r-value = 0.985 ± 0.026) were achieved for the model fitting. The χ^2-test showed that the fittings of the measured tissue time-activity curves by the two-compartment model were within the 95% confidence level. The mean significant levels ranged from 12.7% for the baseline studies to 6.4% for the xylazine and occlusion studies. Although the quality of fit in studies with lower counts (occlusion and xylazine studies) tended to be not as tight as in all other study groups, the differences in the goodness of fit did not achieve statistical significance (Table 3). The randomness of the data point distribution about the fitted curve was tested by the nonparametric run test (22). In brief, the run test detects serial patterns in a run of numbers. In this study, it was applied to test whether the measured tissue time-activity data points fluctuated in a random fashion above and below the fitted curves. The hypothesis of randomness could not be rejected for all studies, and the mean significant level ranged from 10% for the baseline studies to 5% for all other studies.

MVO_2 in our studies was calculated using the values of tissue concentrations of labeled glutamate, aspartate and TCA-cycle intermediates for normoxia and ischemia found by Ng et al. (8). The good agreements between model-predicted and measured
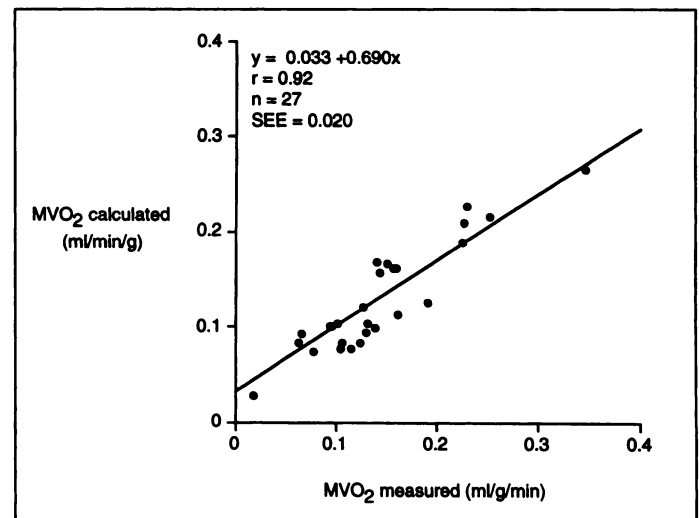
FIGURE 6. Relation between measured and estimated MVO_2 using the two-compartment model. MVO_2 was directly measured using the Fick principle and plotted against model-calculated MVO_2 using the equation in Methods. The data fit well to a linear function over a wide range of MVO_2.

metabolite activities were obtained for the different conditions studied, thus supporting the biochemical validity of the simplified compartment model.

Model Estimates of Spillover and Delay

The model-estimated mean values for spillover and time delay for each group are given in Table 4. The model-estimated spillover fractions (range: 24%–31%) and time delays (range: 0.21–0.33 min.) were not different between the groups.

Model Estimates of Regional MVO_2

The mean values for the model-estimated rate constant k_2 for each group are listed in Table 4. A wide range of MVO_2 (0.02–0.35 ml/min/g) was achieved with the interventions used. Calculated MVO_2 using the equation shown above, under Methods, and measured MVO_2 by the Fick method were correlated in a linear fashion. However, the calculated MVO_2 systematically underestimated measured MVO_2 by approximately 30% (y = 0.033 + 0.690x) as shown in Figure 6. The difference between measured and estimated MVO_2 could be explained by differences in pool sizes for amino acids and TCA intermediates between dogs and rats (i.e., interspecies difference). It is important to note that while concentrations of the individual substrates used to calculate MVO_2 as given in the equation shown above, under Methods, changed over time or under different study conditions, the sum of these substrates remained fairly constant (8).

DISCUSSION

The results of this study demonstrate that a simple compartment model for $[1-^{11}C]$acetate can be used noninvasively to derive estimates of MVO_2. Although the previously used approach with mono- or biexponential curve fitting to determine the rate constant of oxidative metabolism has been proven useful, this new model approach has several advantages.

First, the uptake and clearance of a tracer in the myocardium depend on the shape of the arterial input function that can be altered by the rate of tracer injection or by changes in cardiac output. As shown by computer simulations (6), the monoexponential fitting to the tissue time-activity curve for a given MVO_2 can be significantly affected by the shape of the arterial input function, and variations of k_{mono} might be misinterpreted as differences in MVO_2. This compartment model, however, takes differences of the arterial input function into account and should yield the same results regardless of the arterial input function shape. However, the theoretical advantage of the proposed compartment model needs to be investigated further in humans by comparing directly measured MVO_2 to estimated MVO_2.

A second advantage is the automated analysis regardless of the arterial input function (6). Although the monoexponential curve fitting is a simple and, in most cases, very reliable procedure, it depends on the correct choice of the data points used, which renders the approach somewhat subjective. Curve fitting or choosing data points on the time-activity curve can be especially difficult or even impossible when the time-activity curves are noisy (i.e., studies with low counting rates). Third, the compartment model can be used to estimate absolute regional MVO_2 rather than indices of oxidative metabolism or rate constants, provided that data for correction of the arterial input function exist and the amount of substrate available, in other words, pool sizes for oxidation intermediates through the TCA cycle, is known.

In order to use the proposed tracer kinetic model, the $[1-^{11}C]$acetate concentration in arterial blood (i.e., the true input function) needs to be determined by serial blood samples.

Although $[1-^{11}C]$acetate is the major component of the input function early after tracer administration, other components such as amino acids, TCA cycle intermediates and CO_2 contribute to the input function later on (Fig. 4). Thus, the acquisition of these metabolite concentrations is essential for accurate estimations of myocardial blood flow and MVO_2. However, possible species-related differences in metabolic rates of acetate may require a separate database for metabolite correction. Consistent with such possible species-related differences is the observation that clearance rates of $[1-^{11}C]$acetate for a given rate pressure product are higher in dogs than in humans (2,11). These differences may be attributable to possible differences in metabolite pool sizes between dogs and humans.

In order for the proposed compartment model to be valid, it is assumed that the tissue metabolite pool sizes remain rather stable under different conditions as reported in previous studies. For example, a large decrease in cardiac work by KCl arrest has essentially no effect on glutamate and aspartate pool sizes, and although the citrate pool increases fourfold, this would have little effect relative to the large amino acid pools (25). In another study, the addition of 5 mM acetate led to an increase in the glutamate and citrate pools, but this was offset by decreased aspartate levels so that the total pool size remained unchanged (14).

Spillover and time delay are the two major error sources in dynamic PET studies. In general, spillover poses a problem in the earlier time points when activity in the left ventricular blood pool is high (i.e., spillover from blood to myocardium). One method to correct for spillover is based on the geometry of the myocardium (26,27) that means it is done before the model fitting. Spillover can also be treated as a separate model parameter in addition to those used for the curve fitting or given as a prior parameter (27,28). Spillover correction in the model approach can be done either before or during model fitting (19). Delay denotes the difference in tracer arrival times between the left ventricular cavity (measured activity) and myocardial tissue (nonobservable activity). Like spillover, delay can be corrected for either before or during model fitting. The latter approach, which has been used for all our studies, has been described previously for the tracer $H_2^{15}O$ in brain-flow measurements (19).

Study Limitations

The most important limitation of this study is the lack of directly measured pool sizes of metabolites. Estimates of absolute MVO_2 in this study are based on pool sizes for amino acids and TCA-cycle intermediates determined in rats. These pool sizes may indeed differ from those in dogs that may account for the systematic underestimation of MVO_2. Furthermore, little is known about the influence of pharmacological and surgical interventions on uptake and metabolism of acetate and possible changes in pool size. As stated previously, direct measurements of tissue concentrations are labor-intensive and expensive, and the current study was only performed to investigate whether the proposed simplifications and assumptions can hold in an in vivo environment and whether the simplified model is workable. However, the highly significant linear correlation between measured and estimated MVO_2 implies that accurate estimates are indeed feasible.

CONCLUSION

The findings of this study indicate that MVO_2 can be estimated noninvasively with intravenous $[1-^{11}C]$acetate, dynamic PET imaging and with a simple compartment model,

provided that the amount of substrate available for TCA-cycle oxidation is known. Different input function shapes can be taken into account by a simple tracer kinetic model that might be important in patient studies with severely reduced left ventricular function. Further studies in humans are under way to evaluate the clinical use of this compartment model.

ACKNOWLEDGMENTS

REFERENCES

1. Buxton DB, Schwaiger M, Nguyen A, Phelps ME, Schelbert HR. Radiolabeled acetate as a tracer of myocardial tricarboxylic acid cycle flux. *Circ Res* 1988;63:628–634.
2. Armbrecht JJ, Buxton DB, Brunken RC, Phelps ME, Schelbert HR. Regional myocardial oxygen consumption determined noninvasively in humans with [1-^{11}C]acetate and dynamic positron tomography. *Circulation* 1989;80:863–872.
3. Armbrecht JJ, Buxton DB, Schelbert HR. Validation of [1-^{11}C]acetate as a tracer for noninvasive assessment of oxidative metabolism with positron emission tomography in normal, ischemic, post-ischemic and hyperemic canine myocardium. *Circulation* 1990;81:1594–1605.
4. Brown MA, Myears DW, Bergmann SR. Noninvasive assessment of canine myocardial oxidative metabolism with ^{11}C-acetate and positron emission tomography. *J Am Coll Cardiol* 1988;12:1054–1063.
5. Brown MA, Myears DW, Bergmann SR. Validity of estimates of myocardial oxidative metabolism with carbon-11-acetate and positron emission tomography despite altered patterns of substrate utilization. *J Nucl Med* 1989;30:187–193.
6. Chen K, Sun KT, Buxton DB, Hansen HW, Schelbert HR, Huang SC. The effect of plasma time-activity curve shape on estimates of myocardial oxygen consumption rate with C-11-acetate studies [Abstract]. *J Nucl Med* 1993;34:50 P.
7. Buck A, Wolpers H, Hutchins G, Savas V, Mangner T, Nguyen N. Effect of carbon-11-acetate recirculation on estimates of myocardial oxygen consumption by PET. *J Nucl Med* 1991;32:1950–1957.
8. Ng CK, Huang SC, Schelbert HR, Buxton DB. Validation of a model for

9. Heymann MA, Payne BD, Hoffman JIE, Rudolph AM. Blood-flow measurements with radionuclide-labeled particles. *Prog Cardiovasc Dis* 1977;20:55–79.
10. Pike VW, Eakins MN, Allan RM, Selwyn AP. Preparation of [1-11C]acetate—an agent for the study of myocardial metabolism by positron emission tomography. *Int J Appl Radiat* 1982;33:505–512.
11. Buxton DB, Nienaber CA, Luxen A, Ratib O, Hansen H, Phelps ME. Noninvasive quantitation of regional myocardial oxygen consumption in vivo with [1-11C]acetate and dynamic positron emission tomography. *Circulation* 1989;79:134–142.
12. Fick A. Ueber die Messung des Blutquantums in den Herzventrikeln. *Sitzungen der Physikalisch-Medizinischen Gesellschaft Würzburg* 1870:16.
13. Buffington CK, De Buysere MS, Olson MS. Studies on the regulation of the branched chain a-keto acid dehydrogenase in the perfused rat heart. *J Biol Chem* 1979;254: 10453–10458.
14. Randle PJ, England PJ, Denton RM. Control of the tricarboxylate cycle and its interaction with glycolysis during acetate utilization in rat hearts. *Biochem J* 1970; 117:677–695.
15. Kuhle W, Porenta G, Huang S-C, Phelps M, Schelbert H. Issues in the quantitation of reoriented cardiac PET images. *J Nucl Med* 1992;33:1235–1242.
16. Porenta G, Kuhle W, Sinha S, Krivokapich J, Czernin J, Gambhir S. Gated PET FDG imaging permits parameter estimation of cardiac geometry: validation using gated MR imaging and echocardiography [Abstract]. *J Nucl Med* 1991;32:927.
17. Phelps ME, Huang SC, Hoffman EJ, Selin C, Sokoloff L, Kuhl DE. Tomographic measurement of local cerebral glucose metabolic rate in humans with (F-18) 2-fluoro-2-deoxy-D-glucose: validation of method. *Ann Neurol* 1979;6:371–388.
18. Fletcher R. *Practical methods of optimization*, vol 2. Chichester, NY: John Wiley and Sons; 1980.
19. Meyer E. Simultaneous correction for tracer arrival delay and dispersion in CBF measurements by the H$_2$^{15}O autoradiographic method and dynamic PET. *J Nucl Med* 1989;30:1069–1078.
20. Press WH, Teukolsky SA, Vetterling WT, Flannery BP. *Numerical recipes in C*, 2nd ed. New York: Cambridge University Press; 1992.
21. Landaw E, Distefano III J. Multiexponential, multicompartmental and noncompartmental modeling. II. Data analysis and statistical considerations. *Am J Physiol* 1984;246:R665–R677.
22. Ghulam W. Runs test of randomness with more than two types of elements [Dissertation]. Tempe, AZ: Arizona State University; 1989.
23. Neter J, Wasserman W, Kutner MH, eds. *Applied linear statistical models: regression, analysis of variance and experimental designs*, 3rd ed. Boston, MA: Irwin; 1990.
24. Huang SC, Barrio JR, Yu D-C, Chen B, Grafton S, Melega WP. Modelling approach for separating blood time-activity curves in positron emission tomographic studies. *Phys Med Biol* 1991;36:749–761.
25. Peuhkurinen KJ, Nuutinen EM, Pietiläinen EP, Hiltunen JK, Hassinen IE. Role of pyruvate carboxylation in the energy-linked regulation of pool sizes of tricarboxylic acid-cycle intermediates in the myocardium. *Biochem J* 1982;208:577–581.
26. Henze E, Huang SC, Ratib O, Hoffman E, Phelps ME, Schelbert HR. Measurements of regional tissue and blood pool radiotracer concentrations from serial tomographic images of the heart. *J Nucl Med* 1983;24:987–996.
27. Bergmann SR, Herrero P, Markham J, Weinheimer CJ, Walsh MN. Noninvasive quantitation of myocardial blood flow in human subjects with oxygen-15-labeled water and positron emission tomography. *J Am Coll Cardiol* 1989;14:639–652.
28. Huang SC, Grover M, Hoffman EJ, Schelbert HR, Phelps ME. Use of temporal information for spillover correction in dynamic PET studies of the heart [Abstract]. *J Nucl Med* 1986;27:980.

[1-11C]acetate as a tracer of cardiac oxidative metabolism. *Am J Physiol* 1994;266: H1304–H1315.